International Scholarly Research Network
ISRN Nanomaterials
Volume 2012, Article ID 169850, 8 pages
doi:10.5402/2012/169850

Research Article

Si_3N_4 Nanoparticle Addition to Concentrated Magnesium Alloy AZ81: Enhanced Tensile Ductility and Compressive Strength

Muralidharan Paramsothy,[1] Xing He Tan,[2] Jimmy Chan,[2] Richard Kwok,[2] and Manoj Gupta[1]

[1] *Department of Mechanical Engineering, National University of Singapore, 9 Engineering Drive 1, Singapore 117576*
[2] *CTO Office, Singapore Technologies Kinetics Ltd (ST Kinetics), 249 Jalan Boon Lay, Singapore 619523*

Correspondence should be addressed to Muralidharan Paramsothy, mpsothy@yahoo.co.uk

Received 16 October 2012; Accepted 2 November 2012

Academic Editors: A. Datta, G. Jin, and A. Sorrentino

This study is aimed at understanding the tensile ductility and compressive strength-enhancing dual function of nanoparticles in a concentrated magnesium alloy (AZ81) nanocomposite. Si_3N_4 nanoparticles were selected for reinforcement purposes due to the known affinity between magnesium and nitrogen. AZ81 magnesium alloy was reinforced with Si_3N_4 nanoparticles using solidification processing followed by hot extrusion. The nanocomposite exhibited similar grain size and hardness to the monolithic alloy, reasonable nanoparticle distribution, and nondominant (0 0 0 2) texture in the longitudinal direction. Compared to the monolithic alloy in tension, the nanocomposite exhibited higher failure strain (+23%) without significant compromise in strength, and higher energy absorbed until fracture (EA) (+27%). Compared to the monolithic alloy in compression, the nanocomposite exhibited similar failure strain (+3%) with significant increase in strength (up to +20%) and higher EA (+24%). The beneficial effects of Si_3N_4 nanoparticle addition on tensile ductility and compressive strength dual enhancement of AZ81 alloy are discussed in this paper.

1. Introduction

Silicon nitride nanoparticles in the shape of near-spheres and wires have been synthesized by chemical vapor deposition (CVD) [1, 2]. In the case of nanowires, the catalytic properties of metal nanoparticles were utilized during CVD to promote the directed silicon nitride growth at nanoscale [2]. On one hand, nanoparticles are active towards cells (or bioactive), where the specific biological function at cellular level can be disrupted, modified (negatively or positively), or promoted by the uncoated nanoparticles present [3]. On the other hand, silicon nitride nanoparticles have been coated and chemically stabilized prior to effective dispersion in a rubber matrix [4]. In the context of mechanical (crystallographic structure related) or functional (electronic structure related) properties, the function of nanoparticles in a metallic matrix is related to (a) nanoparticle-matrix reactivity and (b) nanoparticle distribution in the matrix. Magnesium alloys are an easily available lightweight and energy saving metallic matrix. In particular, the AZ (Aluminium-Zinc) series of magnesium alloys are characterized by (a) low cost, (b) ease of handling, (c) good strength and ductility, and (d) resistance to atmospheric corrosion [5]. These qualities enable the common use of AZ series magnesium alloys [5]. Regarding magnesium nanocomposites, the friction stir processing technique has been used to add SiO_2 nanoparticles to AZ61 [6]. Here, the tensile elongation at 350°C of selected composites was lower than 100% at $1 \times 10^{-3}\,s^{-1}$ strain rate but reached 350% and 420% at $1 \times 10^{-2}\,s^{-1}$ and $1 \times 10^{-1}\,s^{-1}$ strain rates, respectively. High strain rate superplasticity was exhibited taking into consideration the sufficiently uniform dispersion of SiO_2 nanoparticles. In another case, the superplasticity of Mg-Zn-Zr composite systems containing SiC microparticles or submicroparticles has been studied and attributed to (a) fine grain size (lesser twinning effects) and (b) crystallographic textural effects [7, 8]. Concerning solidification processed magnesium alloy nanocomposites, existing representative research literature indicates that (a) good nanoparticle distribution can be achieved in the magnesium matrix and (b) better mechanical

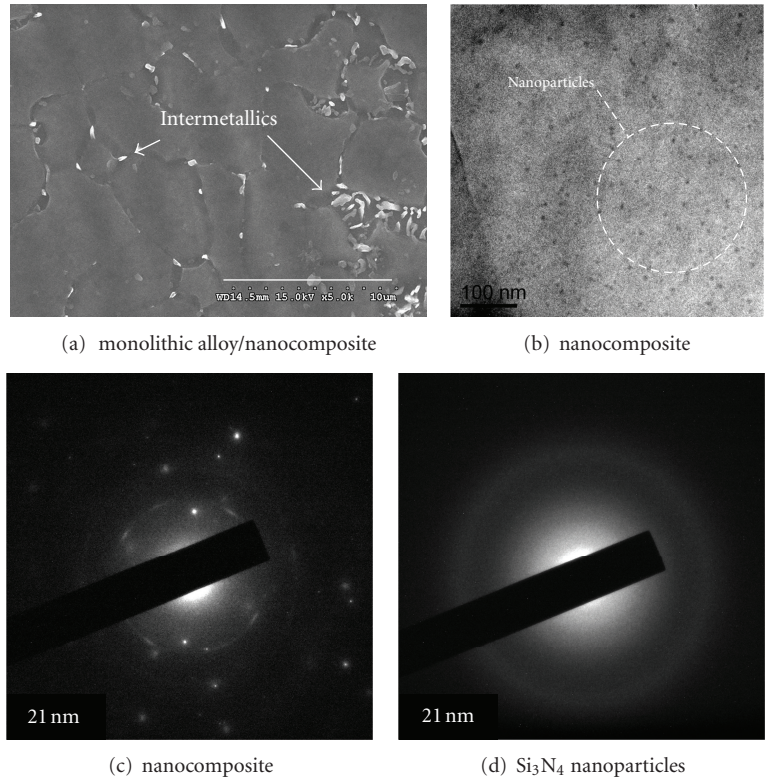

(a) monolithic alloy/nanocomposite (b) nanocomposite

(c) nanocomposite (d) Si_3N_4 nanoparticles

Figure 1: (a) Representative SEM micrograph showing grain size in monolithic AZ81 and AZ81/Si_3N_4 nanocomposite. (b) Representative TEM micrograph showing the presence of individual nanoparticles (fine intermetallics inclusive) in AZ81/Si_3N_4 nanocomposite. Representative SAED diffraction patterns of (c) AZ81/Si_3N_4 nanocomposite and (d) Si_3N_4 nanoparticles. Linked with Table 3. (Prior to tensile/compressive testing).

properties (specifically ductility) can be achieved due to the addition of nanoparticles [9–13].

The physical attributes of second phase precipitates influence the mechanical properties of the alloy. Regarding concentrated AZ series magnesium alloys (e.g., AZ80 and AZ91), the Mg-Al second phase presence significantly contributes to strengthening. Solutionizing heat treatment (where the Mg-Al second phase goes into solution): (a) drastically removes the strengthening effect and (b) significantly contributes to ductility enhancement. Not much is known about the interplay between nanoscale reinforcement presence and second phase precipitation (which is especially relevant in concentrated magnesium alloy nanocomposites) concerning the effects on mechanical properties. Accordingly, this study is aimed at understanding the tensile ductility and compressive strength-enhancing dual function of nanoparticles in an AZ81 alloy nanocomposite. AZ81 was reinforced with Si_3N_4 nanoparticles using solidification processing (disintegrated melt deposition (DMD) [14, 15]) followed by hot extrusion.

2. Results and Discussion

2.1. Synthesis of Monolithic AZ81 and Derived AZ81/Si_3N_4 Nanocomposite. Synthesis of monolithic and nanocomposite materials, the final form being extruded rods, was successfully accomplished with (a) no detectable metal oxidation and (b) no detectable reaction between the graphite crucible and melt. The inert atmosphere used during DMD was effective in preventing oxidation of the Mg melt. No stable carbides of Mg or Al formed due to reaction with the graphite crucible. No macropores or shrinkage cavities were observed in the cast monolithic and nanocomposite materials. No macrostructural defects were observed for extruded rods of monolithic and nanocomposite materials.

2.2. Microstructural Characteristics. Microstructural analysis results revealed that grain size and aspect ratio remained statistically unchanged as shown in Table 1 and Figure 1(a). Distribution of nanoparticles and fine intermetallic particles in the nanocomposite was reasonably uniform as shown in Figure 1(b). Goniometer XRD analysis revealed the presence of Al_3Mg_2 and $Al_{12}Mg_{17}$ intermetallics in monolithic AZ81 and the derived nanocomposite. 3 crystallographic planes corresponding to Mg-Al second phase were detected in AZ81/Si_3N_4 as indicated by TEM SAED phase analysis results listed in Table 2 and shown in Figure 1(c). Texture results are listed in Table 3 and shown in Figure 2. In monolithic AZ81 and the derived nanocomposite, the dominant texture in the transverse and longitudinal directions was $(1\,0\,\bar{1}\,1)$.

2.3. Tensile/Compressive Behavior. The overall results of ambient temperature tensile testing of the extruded materials

Table 1: Results of grain characteristics and microhardness of monolithic AZ81 and derived nanocomposite. (Prior to tensile/compressive testing).

Material	Si_3N_4 (vol.%)	Grain characteristics[a]		Microhardness (HV)
		Size (μm)	Aspect ratio	
AZ81	—	7.6 ± 1.6	1.4	115 ± 6
AZ81/1.5 vol% Si_3N_4	1.50	5.8 ± 1.2	1.5	112 ± 6 (−3)

[a]Based on approximately 100 grains.
( ) Brackets indicate % change with respect to corresponding result of monolithic alloy.

Table 2: Phase detection results of AZ81/Si_3N_4 nanocomposite and Si_3N_4 nanoparticle reinforcement based on selected area electron diffraction (TEM). (Prior to tensile/compressive testing).

k space (nm^{-1})	d (Å)	Phase	Plane	Reference d (Å)	JCPDS card #
AZ81/1.5 vol% Si_3N_4 nanocomposite					
39.40	1.595	$Al_{12}Mg_{17}$	(6 2 2)	1.600	011128
46.00	1.366	Mg	(1 1 2)	1.366	350821
46.22	**1.359**	**Mg_3N_2**	**(7 2 1)**	**1.356**	**350778**
60.86	1.032	Al_3Mg_2	(26 6 6)	1.033	290048
64.53	**0.974**	**Si_3N_4**	**(8 5 1)**	**0.973**	**401129**
66.20	0.949	Mg	(2 0 4)	0.951	350821
71.70	0.876	Mg	(3 0 2)	0.873	350821
75.52	0.832	Mg	(1 0 6)	0.829	350821
78.31	0.802	Al_2Mg	(1 5 6)	0.797	341035
Si_3N_4 nanoparticle reinforcement					
46.15	1.361	β Si_3N_4	(1 1 2)	1.358	331160
73.33	0.857	β Si_3N_4	(3 1 3)	0.856	331160

Table 3: Texture results of monolithic AZ81 and derived nanocomposite based on X-ray diffraction (goniometer). (Prior to tensile/compressive testing).

Material	Section[a]	Plane	Average I/I_{max}[b]
AZ81	T	1 0 $\bar{1}$ 0 prism	0.51
		0 0 0 2 basal	0.15
		1 0 $\bar{1}$ 1 pyramidal	**1.00**
	L	1 0 $\bar{1}$ 0 prism	0.31
		0 0 0 2 basal	0.68
		1 0 $\bar{1}$ 1 pyramidal	**1.00**
AZ81/1.5 vol% Si_3N_4	T	1 0 $\bar{1}$ 0 prism	0.40
		0 0 0 2 basal	0.09
		1 0 $\bar{1}$ 1 pyramidal	**1.00**
	L	1 0 $\bar{1}$ 0 prism	0.31
		0 0 0 2 basal	0.71
		1 0 $\bar{1}$ 1 pyramidal	**1.00**

[a]T: transverse, L: longitudinal.
[b]I_{max} is XRD maximum intensity from either prism, basal, or pyramidal planes.

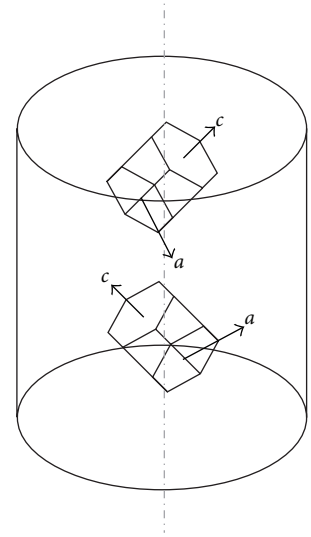

Figure 2: Schematic diagram showing texture of monolithic AZ81 and derived nanocomposite based on goniometer X-ray diffraction. In each case, vertical axis (dotted line) is parallel to extrusion direction. Each cell is made up of 2 HCP units having 1 common (0 0 0 2) basal plane. (Prior to tensile/compressive testing).

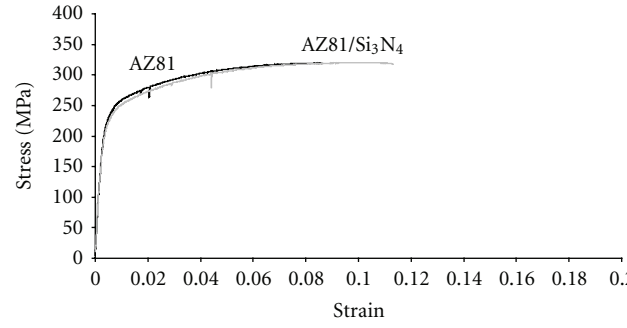

Figure 3: Representative tensile stress-strain curves of monolithic AZ81 and AZ81/Si_3N_4 nanocomposite.

are shown in Table 4 and Figure 3. The overall results of ambient temperature compressive testing of the extruded materials are shown in Table 5 and Figure 4. The tensile failure strain increase in the nanocomposite compared to the corresponding monolithic alloy can be attributed to the following factors (pertaining to reinforcement) (a) presence and reasonably uniform distribution of ceramic nanoparticles [16, 17] and (b) Si_3N_4 nanoparticle induced regulated precipitation of Mg-Al second phase as illustrated in Figure 5. Regarding factor (a), it has been shown in previous studies that the nanoparticles provide sites where cleavage cracks are opened ahead of the advancing crack

Table 4: Results of tensile testing of monolithic AZ81 and derived nanocomposite. Linked with Figure 3.

Material	0.2% TYS (MPa)	UTS (MPa)	Failure strain (%)	Energy absorbed, EA (MJ/m^3)[a]
AZ81	227 ± 3	321 ± 2	8.7 ± 0.9	26 ± 3
AZ81/1.5 vol% Si_3N_4	229 ± 9 (+1)	328 ± 7 (+2)	10.7 ± 0.9 (+23)	33 ± 3 (+27)

[a]Energy absorbed until fracture that is, area under the engineering stress-strain curve until the point of fracture (obtained using EXCEL software).
( ) Brackets indicate % change with respect to corresponding result of monolithic alloy.

Table 5: Results of compressive testing of monolithic AZ81 and derived nanocomposite. Linked with Figure 4.

Material	0.2% CYS (MPa)	UCS (MPa)	Failure strain (%)	Energy absorbed, EA (MJ/m^3)[a]
AZ81	93 ± 7	510 ± 19	19.9 ± 2.7	74 ± 9
AZ81/1.5 vol% Si_3N_4	112 ± 19 (+20)	543 ± 5 (+6)	20.5 ± 1.3 (+3)	92 ± 9 (+24)

[a]Energy absorbed until fracture that is, area under the engineering stress-strain curve until the point of fracture (obtained using EXCEL software).
( ) Brackets indicate % change with respect to corresponding result of monolithic alloy.

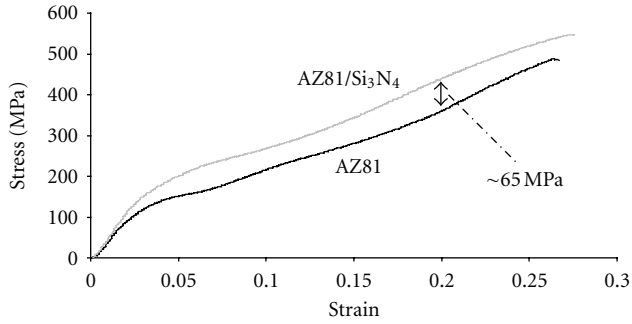

Figure 4: Representative compressive stress-strain curves of monolithic AZ81 and AZ81/Si_3N_4 nanocomposite.

front. This (1) dissipates the stress concentration which would otherwise exist at the crack front and (2) alters the local effective stress state from plane strain to plane stress in the neighbourhood of the crack tip [16, 17]. Regarding factor (b), dissolved Al possibly segregated at the liquid-Si_3N_4 nanoparticle interface enabling Mg-Al second phase manipulation at the nanoscale. This is similar to possible dissolved Zn segregation at the liquid-SiC nanoparticle interface enabling nanoscale $MgZn_2$ precipitation as recently reported [13]. The Si_3N_4 nanoparticle was originally amorphous in the as-supplied form but adopted a crystalline structure in the nanocomposite as shown in Figures 1(d) and 1(c) (resp.) and listed in Table 2. With a reasonably uniform 1.5 vol% Si_3N_4 distribution throughout the AZ81 matrix, the nanoparticle-matrix interface area was insufficient for effectively regulated segregation of 7.80–9.20 wt% Al (or 5.15–6.13 vol% Al) as nanoscale Mg-Al precipitates. The Si_3N_4 nanoparticle regulated precipitation of Mg-Al second phase is illustrated in Figure 5(c). Generally, while the Si_3N_4 nanoparticle is active in nanoscale manipulation of the Mg-Al second phase, the second phase nanoparticles newly formed move away, allowing more second phase nanoparticles to be formed adjacent to the active Si_3N_4 nanoparticle. This occurs until the Si_3N_4 nanoparticle reacts with the Mg based matrix to form a larger Mg_3N_2 particle (Mg_3N_2 particle formation not shown in Figure 5(c)). 1 crystallographic plane corresponding to Mg_3N_2 was detected in AZ81/Si_3N_4 as indicated by TEM SAED phase analysis results listed in Table 2 and shown in Figure 1(c). Some of the second phase nanoparticles that moved away from the active Si_3N_4 nanoparticle initially to make room also begin to grow larger. When the rate of second phase nanoparticle formation from the active Si_3N_4 nanoparticle exceeds the rate of earlier-formed second phase nanoparticle growth, the fraction of second phase particles of relatively smaller size increases, as illustrated in Figure 5(b) compared to Figure 5(a). In this case of reduction in size of Mg-Al second phase, redistribution of smaller second phase (compare between predominantly aggregated type and dispersed type) assists in improving ductility [18].

Any hypothetical strength increase in the nanocomposite (effect 1) can be attributed to the following well known factors (pertaining to reinforcement): (a) dislocation generation due to elastic modulus mismatch and coefficient of thermal expansion mismatch between the matrix and reinforcement [19–22], (b) Orowan strengthening mechanism [21–23], and (c) load transfer from matrix to reinforcement [19, 21]. However, any hypothetical strength decrease in the nanocomposite (effect 2) can be attributed to reduction in size of Mg-Al second phase (since there is no statistical change in grain size between AZ81 and AZ81/Si_3N_4). In this study, effects 1 and 2 equalled each other in tension, causing the AZ81/Si_3N_4 and AZ81 tensile stress-strain curves to overlap each other as shown in Figure 3. However, effect 1 significantly outweighed effect 2 in compression, causing the AZ81/Si_3N_4 stress-strain curve to be above the AZ81 stress-strain curve (maximum 65 MPa stress difference) as shown in Figure 4. This implied that the AZ81-Si_3N_4 nanoscale interface was relatively less adequate in tension (crack opening deformation) but relatively more adequate in compression (crack closing deformation), as is the case with a less adequate particle-matrix interface in a composite that is unable to fully accommodate the stress concentrating effects associated with crack opening (during tensile deformation)

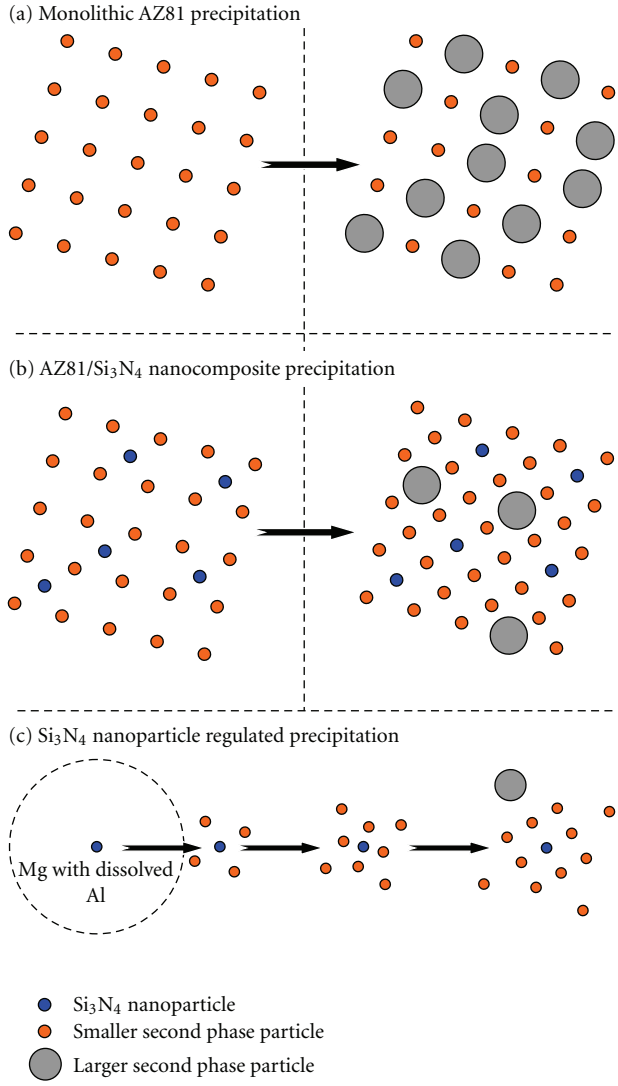

Figure 5: Schematic diagram showing second phase precipitation in (a) monolithic AZ81 and (b) AZ81/Si_3N_4 nanocomposite. (c) Si_3N_4 nanoparticle regulated second phase precipitation in AZ81/Si_3N_4 nanocomposite. The circular shape of the second phase precipitates is only for illustration purposes.

but otherwise functions satisfactorily in the absence of crack opening (during compressive deformation). In both AZ81/Si_3N_4 and monolithic AZ81, 0.2% TYS was about 2.04 and 2.44 times (>2.00) the 0.2% CYS, respectively. Here, the tensile/compressive yield stress anisotropy was despite the crystallographic texture exhibited where $\{1\ 0\ \bar{1}\ 2\}\langle 10\bar{1}1\rangle$-type twinning was activated along the c-axis of the HCP unit cell in Figure 2 with comparatively similar ease in both tension and compression along the c-axis, based on the 45° angle between the c-axis and the vertical axis [24, 25]. The tensile/compressive yield stress anisotropy can be attributed generally to half the strain rate used (less strain hardening) in compressive testing compared to tensile testing. The tensile/compressive yield stress anisotropy was desirably lower in AZ81/Si_3N_4 compared to monolithic AZ81. This can be attributed to the AZ81-Si_3N_4 nanoscale interface being relatively weaker in tension but relatively stronger in compression.

3. Experimental Section

3.1. Materials. The materials used in this study are listed in Table 6. Essentially, AA1050 was added to AZ61 to increase the nominal aluminium content of AZ61 by 2 wt%. All alloy pieces were sectioned to smaller pieces. All oxide and scale surfaces were removed using machining. All surfaces were washed with ethanol after machining. Si_3N_4 nanoparticles were used as the reinforcement phase in AZ81 magnesium alloy.

3.2. Processing. The monolithic alloys were cast using the DMD method [14, 15]. This involved heating AZ61 and

Table 6: Materials selected for this study.

Material	Available description and/or composition (wt%)	Particle size (nm)	Source
	Alloys		
AZ61	Nominally 5.8–7.2 wt.% Al, 0.15–0.50 wt.% Mn, 0.04–1.50 wt.% Zn, 0.10 wt.% Si max, 0.05 wt.% Cu max, 0.005 wt.% Ni max, 0.005 wt.% Fe max, 0.30 wt.% others max, balance Mg	—	Tokyo Magnesium Co. Ltd., Yokohama, Japan
AA1050	Nominally >99.5 wt.% Al	—	Alfa Aesar, Massachusetts, USA
	Nanoparticle reinforcement		
Si_3N_4	98.5+% purity	15–30	Nanostructured & Amorphous Materials Inc, Texas, USA

Please note that AZ61 is a magnesium alloy while AA1050 is an aluminium alloy.

AA1050 pieces to 750°C in an inert Ar gas atmosphere in a graphite crucible using a resistance heating furnace. The crucible was equipped with an arrangement for bottom pouring. Upon reaching the superheat temperature, the molten slurry was stirred for 2.5 min at 460 rpm using a twin blade (pitch 45°) mild steel impeller to facilitate the uniform distribution of heat. The impeller was coated with Zirtex 25 (86% ZrO_2, 8.8% Y_2O_3, 3.6% SiO_2, 1.2% K_2O and Na_2O, and 0.3% trace inorganics) to avoid iron contamination of the molten metal. The melt was then released through a 10 mm diameter orifice at the base of the crucible. The melt was disintegrated by two jets of argon gas oriented normal to the melt stream located 265 mm from the melt pouring point. The argon gas flow rate was maintained at 25 lpm. The disintegrated melt slurry was subsequently deposited onto a metallic substrate located 500 mm from the disintegration point. An ingot of 40 mm diameter was obtained following the deposition stage. To form the AZ81/1.5 vol% Si_3N_4 alloy nanocomposite, Si_3N_4 nanoparticle powder was isolated by wrapping in Al foil of minimal weight (<0.50 wt% with respect to the total matrix weight) and arranged on top of the alloy blocks with all other DMD parameters unchanged. All billets were machined to 35 mm diameter and hot extruded using 20.25 : 1 extrusion ratio on a 150 ton hydraulic press. The extrusion temperature was 350°C. The billets were held at 400°C for 60 min in a furnace prior to extrusion. Colloidal graphite was used as a lubricant. Rods of 8 mm were obtained.

3.3. Heat Treatment. Heat treatment was carried out on all extruded sections of AZ81 based material at 200°C for 1 hour using a resistance heating furnace. This selection of temperature and time was made in order to relax the AZ81 alloy matrix without recrystallization softening. The recrystallization temperature of AZ80 magnesium alloy (as the nearest matching commercial alloy in terms of composition following 10% cold work after 1 hour) is 345°C [5]. Prior to heat treatment, the sections were coated with colloidal graphite and wrapped in aluminum foil to minimize reaction with oxygen present in the furnace atmosphere.

3.4. Microstructural Characterization. Microstructural characterization studies were conducted on metallographically polished monolithic and nanocomposite extruded samples to determine grain characteristics. Hitachi S4300 Field-Emission SEM was used. Image analysis using Scion software was carried out to determine the grain characteristics. Thin foils were prepared from the nanocomposite extruded samples using disc punch-out and ion-milling for (regarding localized effects): (a) nanoparticle distribution as well as (b) nanoparticle-matrix reactivity observation (based on selected area electron diffraction (SAED)) using transmission electron microscopy (JEOL JEM 3010 TEM with 300 KeV accelerating voltage). Regarding SAED, nanopowder samples of Si_3N_4 (dispersed in ethanol) were also prepared by droplet application onto holey carbon film mounted on copper grids followed by drying. All k-space measurements (k) from SAED patterns were manually obtained and converted to crystallographic lattice d-spacings (d) based on $d = 2\pi/k$. Goniometer XRD studies were conducted using CuK_α radiation ($\lambda = 1.5406$ Å) with a scan speed of 2°/min in an automated Shimadzu LAB-X XRD-6000 diffractometer to determine intermetallic phase(s) presence and dominant textures in the transverse and longitudinal (extrusion) directions (regarding globalised effects). All d-spacings from SAED and goniometer XRD analysis were matched with corresponding d-spacings in the JCPDS database available in the Shimadzu LAB-X XRD-6000 diffractometer operating software to determine all phases present.

3.5. Hardness. Microhardness measurements were made on polished monolithic and nanocomposite extruded samples. Vickers microhardness was measured with an automatic digital Shimadzu HMV Microhardness Tester using 25 gf-indenting load and 15 s dwell time.

3.6. Tensile Testing. Smooth bar tensile properties of the monolithic and nanocomposite extruded samples were determined based on ASTM E8M-05. Round tension test samples of 5 mm diameter and 25 mm gauge length were subjected to tension using a MTS 810 machine equipped with an axial extensometer with a crosshead speed set at 0.254 mm/min.

3.7. Compressive Testing. Compressive properties of the monolithic and nanocomposite extruded samples were determined based on ASTM E9-89a. Samples of 8 mm length (l) and 8 mm diameter (d) where $l/d = 1$ were subjected

to compression using a MTS 810 machine with 0.005 min^{-1} strain rate.

4. Conclusions

(1) Monolithic AZ81 and the AZ81/Si_3N_4 nanocomposite can be successfully synthesized using the DMD technique followed by hot extrusion.

(2) In tension, the AZ81/Si_3N_4 nanocomposite stress-strain curve was overlapping the AZ81 curve. In compression, the AZ81/Si_3N_4 nanocomposite stress-strain curve was above the AZ81 curve. This can be attributed to the AZ81-Si_3N_4 nanoscale interface being relatively less adequate in tension (crack opening deformation) but relatively more adequate in compression (crack closing deformation). In both cases, reduction in size of Mg-Al second phase supported hypothetical decrease in strength.

(3) The tensile failure strain increase in the AZ81/Si_3N_4 nanocomposite compared to monolithic AZ81 can be attributed to the following factors (pertaining to reinforcement): (a) presence and reasonably uniform distribution of ceramic nanoparticles and (b) Si_3N_4 nanoparticle induced regulated precipitation of Mg-Al second phase.

(4) The AZ81/Si_3N_4 nanocomposite exhibited higher tensile and compressive energy absorbed until fracture (EA) compared to monolithic AZ81.

Acknowledgments

The authors wish to acknowledge National University of Singapore (NUS) and Temasek Defence Systems Institute (TDSI) for funding this research (TDSI/09-011/1A and WBS # R265000349).

References

[1] C.-S. Kim, W.-K. Youn, D.-K. Lee, K.-S. Seol, and N.-M. Hwang, "Low-temperature deposition of crystalline silicon nitride nanoparticles by hot-wire chemical vapor deposition," *Journal of Crystal Growth*, vol. 311, no. 15, pp. 3938–3942, 2009.

[2] H. Y. Kim, J. Park, and H. Yang, "Synthesis of silicon nitride nanowires directly from the silicon substrates," *Chemical Physics Letters*, vol. 372, no. 1-2, pp. 269–274, 2003.

[3] Y. F. Zhang, Y. F. Zheng, and L. Qin, "A comprehensive biological evaluation of ceramic nanoparticles as wear debris," *Nanomedicine: Nanotechnology, Biology, and Medicine*, vol. 7, no. 6, pp. 975–982, 2011.

[4] Y. Tai, J. Miao, J. Qian, R. Xia, and Y. Zhang, "An effective way to stabilize silicon nitride nanoparticles dispersed in rubber matrix by a one-step process," *Materials Chemistry and Physics*, vol. 112, no. 2, pp. 659–667, 2008.

[5] M. M. Avedesian and H. Baker, *ASM Specialty Handbook: Magnesium and Magnesium Alloys*, ASM International, Materials Park, Ohio, USA, 1999.

[6] C. J. Lee, J. C. Huang, and P. J. Hsieh, "Mg based nanocomposites fabricated by friction stir processing," *Scripta Materialia*, vol. 54, no. 7, pp. 1415–1420, 2006.

[7] Y. Feng, X. Zhou, Z. Min, and W. Kun, "Superplasticity and texture of SiC whiskers in a magnesium-based composite," *Scripta Materialia*, vol. 53, no. 3, pp. 361–365, 2005.

[8] T. G. Nieh, A. J. Schwartz, and J. Wadsworth, "Superplasticity in a 17 vol.% SiC particulate-reinforced ZK60A magnesium composite (ZK60/SiC/17p)," *Materials Science and Engineering A*, vol. 208, no. 1, pp. 30–36, 1996.

[9] M. Paramsothy, S. F. Hassan, N. Srikanth, and M. Gupta, "Enhancing tensile/compressive response of magnesium alloy AZ31 by integrating with Al_2O_3 nanoparticles," *Materials Science and Engineering A*, vol. 527, no. 1-2, pp. 162–168, 2009.

[10] M. Paramsothy, S. F. Hassan, N. Srikanth, and M. Gupta, "Simultaneous enhancement of tensile/compressive strength and ductility of magnesium alloy AZ31 using carbon nanotubes," *Journal of Nanoscience and Nanotechnology*, vol. 10, no. 2, pp. 956–964, 2010.

[11] M. Paramsothy, J. Chan, R. Kwok, and M. Gupta, "Enhanced mechanical response of hybrid alloy AZ31/AZ91 based on the addition of Si_3N_4 nanoparticles," *Materials Science and Engineering A*, vol. 528, no. 21, pp. 6545–6551, 2011.

[12] M. Paramsothy, J. Chan, R. Kwok, and M. Gupta, "TiC nanoparticle addition to enhance the mechanical response of hybrid magnesium alloy," *Journal of Nanotechnology*, vol. 2012, Article ID 401574, 9 pages, 2012.

[13] M. De Cicco, H. Konishi, G. Cao et al., "Strong, ductile magnesium-zinc nanocomposites," *Metallurgical and Materials Transactions A*, vol. 40, no. 12, pp. 3038–3045, 2009.

[14] L. M. Tham, M. Gupta, and L. Cheng, "Influence of processing parameters during disintegrated melt deposition processing on near net shape synthesis of aluminium based metal matrix composites," *Materials Science and Technology*, vol. 15, no. 10, pp. 1139–1146, 1999.

[15] M. Gupta, M. O. Lai, and S. C. Lim, "Regarding the processing associated microstructure and mechanical properties improvement of an Al–4.5 Cu alloy," *Journal of Alloys and Compounds*, vol. 260, no. 1-2, pp. 250–255, 1997.

[16] S. F. Hassan and M. Gupta, "Effect of particulate size of Al_2O_3 reinforcement on microstructure and mechanical behavior of solidification processed elemental Mg," *Journal of Alloys and Compounds*, vol. 419, no. 1-2, pp. 84–90, 2006.

[17] S. F. Hassan and M. Gupta, "Development of nano-Y_2O_3 containing magnesium nanocomposites using solidification processing," *Journal of Alloys and Compounds*, vol. 429, no. 1-2, pp. 176–183, 2007.

[18] G. E. Dieter, *Mechanical Metallurgy*, McGraw-Hill, London, UK, SI Metric edition, 1998.

[19] S. F. Hassan and M. Gupta, "Effect of different types of nano-size oxide participates on microstructural and mechanical properties of elemental Mg," *Journal of Materials Science*, vol. 41, no. 8, pp. 2229–2236, 2006.

[20] S. F. Hassan and M. Gupta, "Enhancing physical and mechanical properties of Mg using nanosized Al_2O_3 particulates as reinforcement," *Metallurgical and Materials Transactions A*, vol. 36, no. 8, pp. 2253–2258, 2005.

[21] Z. Száraz, Z. Trojanová, M. Cabbibo, and E. Evangelista, "Strengthening in a WE54 magnesium alloy containing SiC particles," *Materials Science and Engineering A*, vol. 462, no. 1-2, pp. 225–229, 2007.

[22] L. H. Dai, Z. Ling, and Y. L. Bai, "Size-dependent inelastic behavior of particle-reinforced metal-matrix composites," *Composites Science and Technology*, vol. 61, no. 8, pp. 1057–1063, 2001.

[23] D. Hull and D. J. Bacon, *Introduction to Dislocations*, Butterworth-Heinemann, Oxford, UK, 4th edition, 2002.

[24] T. Laser, C. Hartig, M. R. Nürnberg, D. Letzig, and R. Bormann, "The influence of calcium and cerium mischmetal on the microstructural evolution of Mg–3Al–1Zn during extrusion and resulting mechanical properties," *Acta Materialia*, vol. 56, no. 12, pp. 2791–2798, 2008.

[25] J. Bohlen, S. B. Yi, J. Swiostek, D. Letzig, H. G. Brokmeier, and K. U. Kainer, "Microstructure and texture development during hydrostatic extrusion of magnesium alloy AZ31," *Scripta Materialia*, vol. 53, no. 2, pp. 259–264, 2005.